Tailoring of magnetism in Pt/Co/Pt ultrathin films by ion irradiation

A. Maziewski,[1,*] P. Mazalski,[1] Z. Kurant,[1] M. O. Liedke,[2] J. McCord,[2,3] J. Fassbender,[2] J. Ferré,[4] A. Mougin,[4] A. Wawro,[5] L. T. Baczewski,[5] A. Rogalev,[6] F. Wilhelm,[6] and T. Gemming[7]

[1]*University of Białystok, Faculty of Physics, 41 Lipowa str, 15-424 Białystok, Poland*
[2]*Helmholtz-Zentrum Dresden-Rossendorf, 01328 Dresden, Germany*
[3]*Institute for Materials Science, Christian-Albrechts-University of Kiel, 24143 Kiel, Germany*
[4]*Laboratoire de Physique des Solides, UMR CNRS 8502, Université Paris-Sud, 91405, Orsay, France*
[5]*Institute of Physics, Polish Academy of Sciences, 02-668 Warszawa, Poland*
[6]*European Synchrotron Radiation Facility (ESRF), BP 220, 38043 Grenoble Cedex, France*
[7]*Leibniz-Institut für Festkörper- und Werkstoffforschung IFW Dresden e.V., 01171 Dresden, Germany*

(Received 20 January 2012; published 24 February 2012)

Magnetization orientation in Ga^+-irradiated Pt/Co(d_{Co})/Pt ultrathin films can be changed in a controlled way by adjusting the ion fluence, F. Two-dimensional (d_{Co}, F) diagrams of magnetic and magneto-optical properties have been derived. Distinct out-of-plane magnetic anisotropy states with enhanced magneto-optical effects were evidenced for specific (d_{Co}, F) values. This rich behavior originates from two competing mechanisms: intermixing of Co and Pt atoms at the interfaces and the formation of ordered CoPt alloy phases with high magnetic anisotropy. The irradiation-induced effects open novel routes for both tailoring thin-film magnetic and magneto-optical properties and patterning of magnetic nanostructures.

DOI: 10.1103/PhysRevB.85.054427 PACS number(s): 75.70.−i, 61.80.−x, 75.30.Gw, 78.20.Ls

I. INTRODUCTION

Thin-film structures exhibiting perpendicular magnetic anisotropy (PMA) are promising candidates for designing spintronic nano-devices implemented to, e.g., ultrahigh density magnetic storage, fast memory applications, and nanosensors.[1,2] PMA is mostly observed in ultrathin multilayers or alloy films. In Co-based multilayers, the effective magnetic anisotropy depends on the Co-layer thickness since it results from the interplay between the interface and volume contributions. Moreover, it is particularly sensitive to the thickness of adjacent nonmagnetic sandwiching layers.[3] In ultrathin Co layers, interface effects predominate and reinforce PMA. The magnetization reorients from in-plane to out-of-plane direction with decreasing Co thickness, d_{Co}, below a critical thickness, d_{RPT}, defining the so-called reorientation phase transition (RPT).

The magnetic properties of CoPt alloy films are highly sensitive to preparation conditions[4,5] and postgrowth thermal treatment.[6] PMA has been only observed for several CoPt alloy compositions obtained at specific growth temperatures. Their magnetic anisotropy is substantially enhanced in comparison to pure Co layers.[7] Thin films of ordered CoPt alloys with strong PMA can be prepared by various techniques: rf-sputtering,[6] electron beam co-evaporation,[8] or molecular beam epitaxy (MBE).[9] In FePd films, a well-ordered $L1_0$ phase with a huge PMA can be even obtained after postgrowth He^+ ion irradiation.[10–13] In general, ion bombardment modifies the microstructure and chemical ordering of alloys and consequently affects their magnetism. Besides standard "bottom-up" and/or "top-down" patterning approaches and postgrowth thermal treatment, the local ion irradiation provides a unique tool for postgrowth structuring of the magnetic properties.[14,15] In particular, focused ion beam (FIB) irradiation stands as a very promising method to modify locally magnetic properties of continuous films at the nanometer scale.[14] Alternatively, magnetic nanostructures can be fabricated by ion irradiation through a mask or by modifying the overlayer thickness.[15–17]

So far, the study of the magnetic properties of ultrathin magnetic multilayers affected by ion irradiation has been limited to as-grown ultrathin films with initial PMA.[18,19] As an example, Ga^+ ion irradiation induces an out-of-plane to in-plane RPT in Pt/Co(d_{Co})/Pt magnetic films (for $d_{Co} < d_{RPT}$) due to ion intermixing occurring at the Co/Pt interfaces and strain release.[14,20] Only recently, a Ga^+ ion irradiation-induced in-plane to out-of-plane magnetization reorientation has been reported for sputtered Pt/Co($d_{Co} = 2.6$ nm)/Pt films, i.e., with $d_{Co} > d_{RPT}$.[21]

In the present paper we report on the evolution of magnetic properties in Pt/Co(d_{Co})/Pt films under a variable Ga^+ ion irradiation fluence F for d_{Co} varying over a wide thickness range. The two-dimensional (2D) (d_{Co}, Log$F$) diagrams of pertinent physical parameters allow us to identify areas with dominating perpendicular or in-plane anisotropy and to point out an oscillatory behavior between PMA and easy-plane magnetized regions. Observed effects are shown to be correlated with the modified crystalline structure of the sample by ion irradiation.

II. EXPERIMENTAL DETAILS

Epitaxial films were grown by MBE system under a base pressure of 10^{-10} Torr. The deposition process was monitored *in-situ* by reflection high-energy electron diffraction (RHEED) and Auger electron spectroscopy (AES). A 20-nm-thick Mo(110) buffer layer was first grown at 1000 °C on an epi-ready sapphire Al_2O_3(11–20) substrate (8×10 mm^2 in lateral size). It was followed by subsequent room temperature deposition of (i) a 20-nm-thick Pt(111) underlayer, (ii) a Co(0001) magnetic layer (as a wedge with thickness ranging between 0 and 5 nm, or a flat film), and (iii) a 5-nm-thick Pt(111) cover layer (see Fig. 1). The sample used for magneto-optical studies was irradiated with an ion fluence increasing from

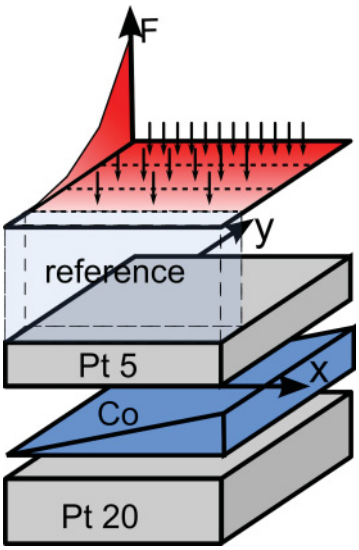

FIG. 1. (Color online) Schematic view of the sample containing the Co wedge like layer. The Ga^+ ions fluence, F, increases with three different gradients along a direction (y) orthogonal to the Co-wedge orientation (x). The thickness of the constituent layers and used fluences are indicated in the text.

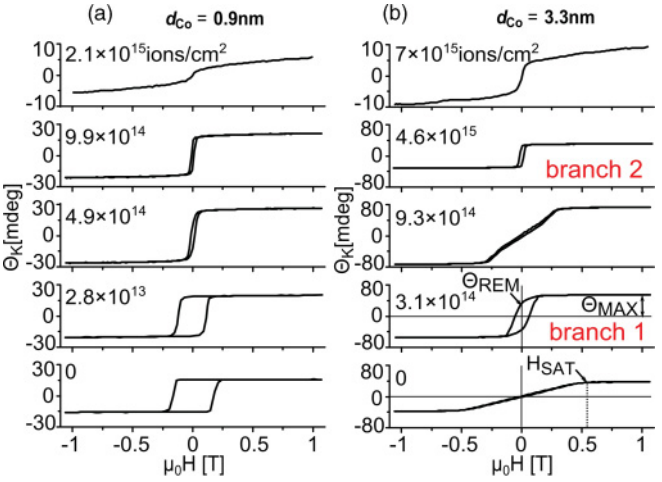

FIG. 2. (Color online) PKR hysteresis loops measured for two selected Co-layer thicknesses: (a) 0.9 nm and (b) 3.3 nm irradiated with the indicated Ga^+ ion fluences. The loops in the upper row (corresponding to the highest fluence) are plotted in a reduced θ_K scale range. Perpendicular square loops appear in branch 1 and branch 2 regions located in the 2D(d_{Co}, Log$F$) diagrams.

10^{13} up to 10^{16} ions/cm^2 along a direction orthogonal to the Co wedge-thickness gradient. The energy (30 keV) of the used Ga^+ ions (leading to a 10 nm mean in-depth implantation) was selected to ensure that they affect the whole film. The fluence was varied across the sample with three different gradients per decade. For a steplike gradient irradiation process, the pattern consisted of 40 uniformly irradiated 73-μm-wide stripes per fluence decade. A non-irradiated part of the sample served as a reference.

Room temperature polar Kerr rotation (PKR) hysteresis loops were measured with a magneto-optical set-up using a laser diode light source (640-nm wavelength) emitting a beam of about 300 μm in diameter. A computer-controlled x-y scanning stage allowed the sample to move relatively to the beam spot to determine the local magnetic and magneto-optical properties of Pt/Co(d_{Co})/Pt over the whole (d_{Co}, Log$F$) range.

Microstructural analyses of the as-deposited and irradiated samples were performed (using FEI Tecnai F30 operating at 300 kV) by high resolution transmission electron microscopy (HRTEM) and analytical scanning transmission electron microscopy (STEM) with high-angle annular dark-field imaging, electron energy loss spectroscopy (EELS), and energy-dispersive x-ray spectroscopy (EDX). Specimen preparation for HRTEM cross-section investigations was done by FIB followed by low-energy Ar-ion milling.

X-ray absorption (XAS) spectra were measured on the ID12 ESRF beamline in Grenoble using the total fluorescence yield detection mode in the presence of a magnetic field of 0.6 T applied at 25° with respect to the normal to the film surface.

III. RESULTS AND DISCUSSION

The hysteresis loops under a magnetic field applied in the perpendicular direction, recorded for two selected Co-layer thicknesses, d_{Co} = 0.9 nm and 3.3 nm, which are well apart from the RPT thickness of the non-irradiated film d_{RPT} = 2.2 nm, are shown in Fig. 2.

A complex F−dependent magnetization behavior is clearly revealed. For the thinner non-irradiated Co layer these loops exhibit a rectangular shape relevant for perpendicularly magnetized films. The gradual increase of F up to 9.9 × 10^{14} ions/cm^2 gives rise to a reduction of the coercivity. For $F >$ 2.1 × 10^{15} ions/cm^2, the field-induced magnetization curve is characteristic for a superparamagnetic behavior. A contrasting evolution of the PKR loop shape occurs for d_{Co} = 3.3 nm > d_{RPT}. When F increases up to 3.1 × 10^{14} ions/cm^2, the magnetization rotates first from an easy-plane to an out-of-plane orientation. At higher fluence, F = 9.3 × 10^{14} ions/cm^2, magnetization falls back again into the film plane. Surprisingly, a further increase of the fluence, up to 4.6 × 10^{15} ions/cm^2, induces again a reorientation of the magnetization towards the out-of-plane direction. Finally, for $F >$ 7 × 10^{15} ions/cm^2, the irradiated sample becomes superparamagnetic.

Five characteristic magnetic and magneto-optical parameters were determined from the hysteresis loops: the maximum PKR, θ_{MAX}; the remanent PKR signal, θ_{REM}; the normalized remanent magnetization, $m_{REM} = \theta_{REM}/\theta_{MAX}$; the coercive field H_C; and the saturation field H_{SAT}. H_{SAT} stands for the effective magnetic anisotropy field of an in-plane magnetized film. The (d_{Co}, Log$F$) contour maps of the dependences of four measured parameters are presented in Fig. 3.

The color representation allows us to locate regions with predominant perpendicular or in-plane alignment of magnetization. Two branches corresponding to (d_{Co}, Log$F$) regions with an out-of-plane magnetization are clearly visible in Figs. 3(a) and 3(b). The fluence dependencies of the relevant magnetic parameters are additionally plotted on both sides of the (d_{Co}, Log$F$) diagrams for d_{Co} = 0.9 nm and 3.3 nm.

For small thicknesses, $d_{Co} < d_{RPT}$, the decrease of the coercive field and normalized remanence with F is observed

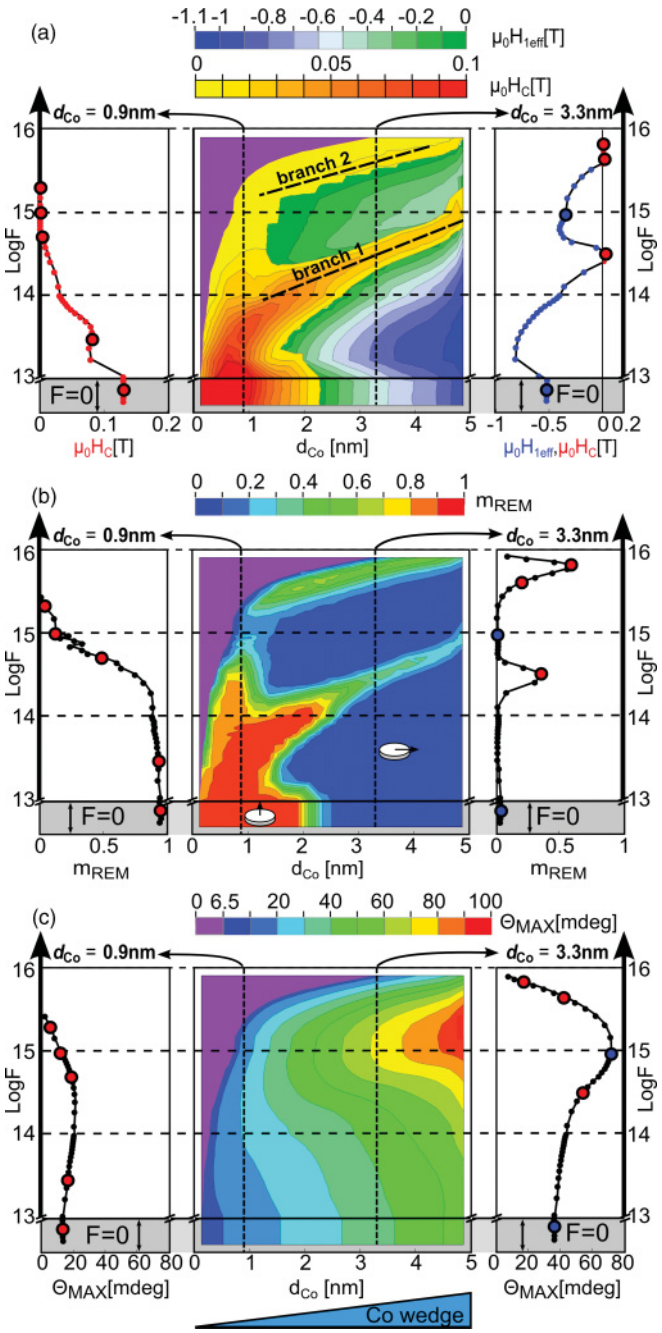

FIG. 3. (Color) Two-dimensional (d_{Co}, Log$F$) diagrams of the magnetic and magneto-optical parameters determined from the PKR loops: (a) coercive field, H_C, and effective anisotropy field, H_{1eff}; (b) normalized remanence, m_{REM}; (c) PKR saturation value, Θ_{MAX}, measured in $\mu_0 H = 1$ T. The superparamagnetic region (violet area) is visible at the top left corner of the diagrams. The plots of these parameters with Log$F$ are shown for two selected thicknesses of the Co layer: 0.9 nm and 3.3 nm on both sides of the diagrams. The encircled red dots correspond to the loops shown in Fig. 2.

[see Figs. 3(a), 3(b)]. A weak maximum in $H_c(F)$ for $F = 2.8 \times 10^{13}$ Ga^+ ions/cm^2 is related to branch 1 (Fig. 3). For the as-deposited in-plane magnetized samples ($d_{Co} > d_{RPT}$), the magnetization is switched twice from the in-plane to out-of-plane directions and vice versa [Figs. 3(a) and 3(b)] with increasing ion fluence. For $d_{Co} = 3.3$ nm, branches 1 and 2 (Fig. 3) are found for $F_1 \approx 2.5 \times 10^{14}$ ions/cm^2 and $F_2 \approx 5.2 \times 10^{15}$ ions/cm^2, respectively (see also Fig. 2). Five successive RPTs between in-plane and out-of-plane magnetized states are evidenced for 1.5 nm $< d_{Co} <$ 2.0 nm. Moreover, as depicted in Fig. 3(c), the PKR value substantially increases under ion irradiation.

We propose a phenomenological model to explain the dependencies of the effective anisotropy field, H_{1eff}, on the fluence F and Co film thickness, d_{Co}, as depicted in Fig. 3(a). In layered structures, H_{1eff} is expressed as the sum of a thickness-independent volume term, H_{V0}, and a contribution of the interface anisotropy field, $H_{S0} = h_{S0}/d_{Co}$. The magnetic behavior observed for increasing F can be qualitatively interpreted by considering two competitive mechanisms: (i) the decrease of the interface anisotropy[20] according to the simple function $A(F) = \mathrm{Exp}(-F/F_0)$, similar to that proposed to describe the irradiation-induced variation of H_C,[23] and (ii) the creation of PMA followed by its disappearance, characterized by an additional volume term and new interface contributions expressed in the form of the simple Gaussian-type function $B(d_{Co}, \mathrm{Log}F)$:

$$B(d_{Co},\mathrm{Log}F) = \mathrm{Exp}[-\{\mathrm{Log}F - \mathrm{Log}f(d_{Co})\}^2], \qquad (1)$$

where the $f(d_{Co})$ function describes the PMA branch central line in the (d_{Co}, Log$F$) plane. Then the effective anisotropy could be described by the simplified expression:

$$H_{1eff}(d_{Co},\mathrm{Log}F) = H_{V0} + \frac{h_{S0}}{d_{Co}} \times A(\mathrm{Log}F) + \left(H_{VF} + \frac{h_{SF}}{d_{Co}}\right) \times B(\mathrm{Log}F, d_{Co}), \qquad (2)$$

considering that both H_{VF}, h_{SF} are volume and interface contributions, respectively.

For branch 1 a simple approximation of $f_1(d_{Co})$ dependence that gives $\mathrm{Log}f_1(d_{Co}) = a_1 + b_1 d_{Co}$ can be applied over a wide Co-layer thickness range [Fig. 3(a)]. The values $\mu_0 H_{V0} = -1.5$ T and $\mu_0 h_{S0} = 3.3$ T·nm were obtained for the non-irradiated film. The parameters $F_0 \approx 10^{13}$, $\mu_0 H_{VF} \approx 1.1$ T, and $\mu_0 h_{SF} \approx 0.6$ T·nm were determined from the fit of the $H_{1eff}(d_{Co}, \mathrm{Log}F)$ dependence given by Eq. (2), using the aforementioned linear approximation for $\mathrm{Log}f_1(d_{Co})$ and the previously specified values for H_{V0}, h_{S0}.

We also performed TRIDYN[24] simulations to determine the composition profile of the atomic species inside the film, the profile of the kinetic energy losses, and the thickness of the eroded layer versus F and d_{Co}. Examples of such simulations are presented in Fig. 4 for a 3.3-nm-thick Co film for two different fluences corresponding to branches 1 or 2. At low fluence, intermixing of Co and Pt atoms takes mainly place at the interfaces.

The erosion depth, S, of the upper part of the sample was estimated to be equal to 3.5 nm for $F = 5.7 \times 10^{15}$ ions/cm^2, within branch 2. This calculated depth is smaller than the Pt overlayer thickness [Fig. 4(b)]. The removal of both the Pt overlayer and Co layer is only reached for $S = 8.3$ nm for a much higher fluence, $F = 1.4 \times 10^{16}$ ions/cm^2. This maximum fluence is out of the studied range discussed in Fig. 3. For the $d_{Co} = 1$ nm, S is as high as 6 nm for $F = 8.8 \times 10^{15}$

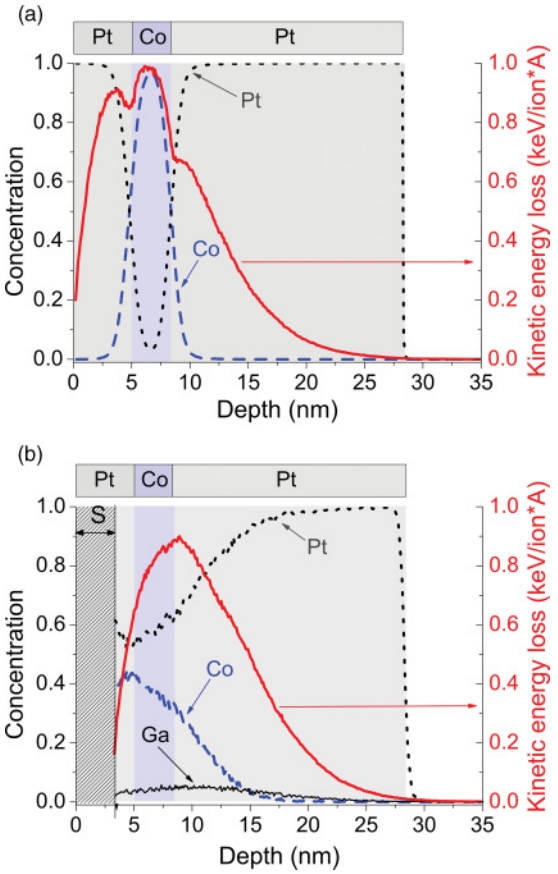

FIG. 4. (Color online) Results of TRIDYN simulations performed for a 30 keV Ga^+ ion irradiation of the Mo(20 nm)/Pt(20 nm)/Co (3.3 nm)/Pt(5 nm) film structure. In-depth composition and kinetic energy losses profiles are calculated for two selected fluences: (a) $F = 2.8 \times 10^{14}$ ions/cm^2 and (b) $F = 5.7 \times 10^{15}$ ions/cm^2. These fluences correspond to the out-of-plane magnetized branches 1 and 2, respectively. The upper-layer thickness, S, removed by irradiation is indicated in the left part of Fig. 4(b) in deep gray. Profiles are marked as follows: point, Pt; dashed line, Co; thin solid line, Ga; thick solid line, energy losses.

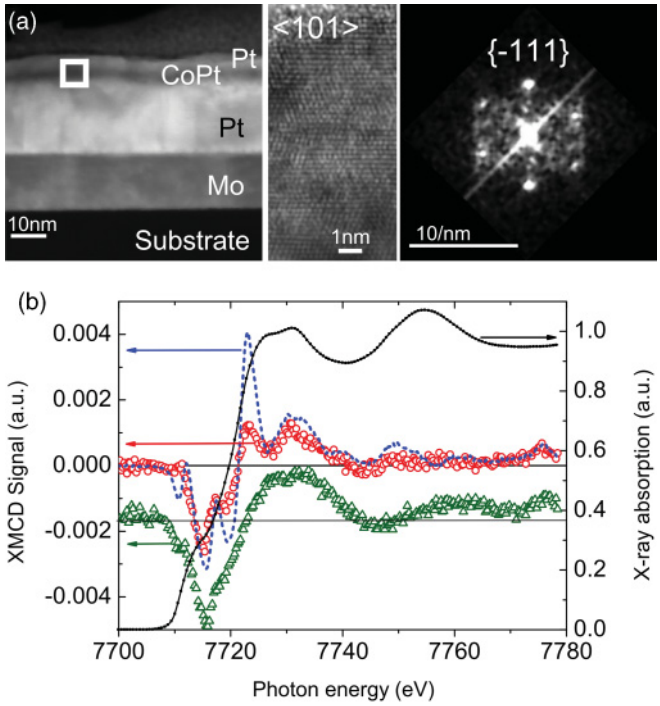

FIG. 5. (Color online) (a) High-angle annular dark-field STEM image (upper left side) of the irradiated sample (branch 1), showing a continuous CoPt layer at the position of the initial Co layer (scale bar 10 nm). A HRTEM-image (upper middle) of this layer region is shown with the corresponding Fourier-transform (upper right side). The position of the HRTEM image is indicated in the STEM image. (b) Room temperature absorption spectrum (XANES) of the Ga^+-irradiated film (branch 1) and Co K-edge XMCD spectra in a magnetic field for the non-irradiated film (triangles), the irradiated film (circles), and CoPt $L1_0$ thin film (dashed line).

ions/cm^2. Then, the erosion depth exceeds the Pt-overlayer thickness, explaining the occurrence of a transition from the ferromagnetic to superparamagnetic state at high fluence.

A mean Pt concentration $\langle x \rangle$ dependence on the fluence in the formed $Co_{1-x}Pt_x$ alloys has been calculated for the sample with $d_{Co} = 3.3$ nm. The value of $\langle x \rangle$ increases quasilogarithmically with F arising from 10^{12} to 10^{16} ions/cm^2. At the initial position of the Co layer (prior to irradiation), $\langle x \rangle$ is found to be close to 0.4 and 0.6 for branches 1 and 2, respectively. It should be emphasized that the real value of $\langle x \rangle$ might be slightly higher because of an initial CoPt intermixing at the interfaces already present in the as-grown sample.[25]

More significant changes of Co and Pt in-depth composition profiles are observed at the higher fluence. In this case Co atoms penetrate deeply both into the Pt underlayer and overlayer, and Pt atoms migrate into the Co layer.

Thus, it is highly probable that the formation of specific alloy compositions, $Co_{0.5}Pt_{0.5}$ ($L1_0$ phase) and $Co_{0.25}Pt_{0.75}$, is responsible for inducing PMA in the branches 1 and 2, respectively. It has been shown that the volume anisotropy of the $Co_{0.5}Pt_{0.5}$ alloy is highly enhanced as compared to pure Co.[26] The effective anisotropy of the $Co_{0.25}Pt_{0.75}$ alloy is expected to increase because of the magnetostatic energy-term reduction.[22] In addition to calculated changes of the chemical composition, chemical forces, not taken into account in TRIDYN simulations, may favor irradiation-driven stabilization of $L1_0$ and $L1_2$ phases.[12] Starting from the previously determined values of H_{VF} and h_{SF}, the fraction of Co ions forming a strong anisotropy phase can be estimated. Assuming the reported magnetic anisotropy contribution of 0.8 meV for a single Co atom in the ordered $L1_0$ phase,[27] the transformation of only 10% of the magnetic film volume into an ordered $L1_0$ phase is enough to fit well the H_{VF} value. A surface anisotropy contribution (independent on the initial Co-layer thickness) equal to 20% of the effective single atomic layer surface is also sufficient to obtain the fitted h_{SF} value.

In order to confirm the previoulsy predicted irradiation-driven structural changes, transmission electron microscopy (TEM) and x-ray magnetic circular dichroism (XMCD) techniques were used. HRTEM cross-section image of a Pt/Co (3.3 nm)/Pt sample uniformly irradiated with the fluence $F = 2.8 \times 10^{14}$ ions/cm^2 (branch 1) shows a clear layered morphology and crystalline structure [see Fig. 5(a)]. The deduced lattice parameter is consistent with that of the ordered

$L1_0$ CoPt alloy. The HRTEM image showing a crystalline structure with some lattice distortions and its Fourier transform indicate that the ⟨101⟩ axis and CoPt {−111} planes are oriented parallel to the surface. From EDX analyses (not shown) a chemical composition close to $Co_{0.5}Pt_{0.5}$ was found at a depth corresponding to the Co-layer position.

Additional information on the presence of $Co_{1-x}Pt_x$ alloys is provided from Co K-edge XAS and XMCD. The Co K-edge XMCD spectrum of the irradiated film with the fluence $F = 2.8 \times 10^{14}$ ions/cm^2 has been compared with that of a similar non-irradiated film and a perfectly ordered $Co_{0.5}Pt_{0.5}$ $L1_0$ thin-film reference alloy grown on a MgO substrate [Fig. 5(b)]. The XMCD spectrum of the as-deposited sample depicts the shape and amplitude typical for pure metallic Co films or nanoparticles.[28,29]

Conversely, the XMCD of the irradiated sample shows a drastically different spectral shape. This confirms that irradiation leads to a significant change of the Co atom's electronic structure due to the different nearest-neighbor configuration, implying the formation of ordered $Co_{1-x}Pt_x$ alloys with enhanced PMA. In order to confirm the presence of a chemically ordered CoPt alloy, we have compared the XMCD spectrum of the irradiated sample [Fig. 5(b)] to that of an ordered $Co_{0.5}Pt_{0.5}$ $L1_0$ thin-film reference sample. There are striking similarities between these two spectra even though the amplitudes of some spectral features are slightly different. However, all the characteristic peaks are present in both spectra at exactly the same energies. Therefore, we interpret the XMCD spectrum of the irradiated sample as the superposition of pure Co and $L1_0$ $Co_{0.5}Pt_{0.5}$ alloy contributions. Analyses of both HRTEM and XMCD results indicate consistently the presence of a highly anisotropic, $L1_0$-ordered CoPt alloy in the Ga^+-irradiated Pt/Co(3.3 nm)/Pt film for branch 1.

IV. CONCLUSION

In conclusion the ability to tailor the magnetic anisotropy, remanence, Kerr rotation, and coercivity in Pt/Co/Pt films by Ga^+-ion irradiation was investigated for a wide range of Co-layer thicknesses. Whereas any postgrowth treatment, so far reported, usually shifts, smears, or suppresses the RPTs, we have demonstrated that ion irradiation affects the chemical and topological film structure inducing multiple oscillatory RPTs. Therefore, an appropriate optimization of ion-irradiation conditions could allow one to pattern nanoscale regions with large PMA surrounded by in-plane anisotropy areas. Observed multiple RPTs result from the competition between two processes: the intermixing at Co/Pt interfaces and the formation of ordered $Co_{1-x}Pt_x$ alloys exhibiting the high out-of-plane magnetic anisotropy. Hence, previously and separately evidenced interface[18] and volume[12] effects are found to coexist here in a given system. Such rich irradiation-induced behavior is not limited merely to MBE-grown films discussed in this paper. We have recently found that Pt/Co/Pt sputtered films deposited on sapphire or on Si/SiN substrates irradiated either by a uniform ion beam or by FIB also show two similar branches in a 2D (d_{Co}, F) diagram with enhanced out-of-plane magnetic anisotropy. At first unexpected, two similar branches with increased anisotropy field were evidenced in Pt/Co/Pt films, irradiated with light He^+ ions. Therefore, the present trends are more general and not limited to a specific preparation technique or ion irradiation procedure. Ion-induced PMA is expected to be present in a wide range of magnetic thin film systems. The Ga^+ irradiation-driven modification of magnetic properties presented in this study is especially promising for designing high resolution patterned planar nanostructures with PMA. This method can be extended to three-dimensional magnetic patterning using variable magnetic layer coverage (chemical composition and/or thickness) and/or ion energy. This offers novel routes for tailoring magnetic anisotropy and other magnetic properties, in particular for designing new media for future spintronic devices.

ACKNOWLEDGMENTS

This work was supported by the Marie-Curie ToK NANOMAG-LAB project (No. MTKD-CT-2004-003177), the Polish-German DAAD-PPP program, and the European Community as an Integrating Activity 'Support of Public and Industrial Research Using Ion Beam Technology (SPIRIT)' under EC contract No. 227012, FANTOMAS project (EC FP7, Grant No. 214810) and ESRF/73/2006 project. We also thank G. Schmerber (IPCMS, Strasbourg, France) for providing the ordered $L1_0$ $Co_{0.5}Pt_{0.5}$ thin film reference sample.

*magnet@uwb.edu.pl

[1] N. Nishimura, T. Hirai, A. Koganei, T. Ikeda, K. Okano, Y. Sekiguchi, and Y. Osada, J. Appl. Phys. **91**, 5246 (2002).

[2] S. Ikeda, K. Miura, H. Yamamoto, K. Mizunuma, H. D. Gan, M. Endo, S. Kanai, J. Hayakawa, F. Matsukura, and H. Ohno, Nat. Mater. **9**, 721 (2010).

[3] M. Kisielewski, A. Maziewski, M. Tekielak, A. Wawro, and L. T. Baczewski, Phys. Rev. Lett. **89**, 087203 (2002) (and references therein).

[4] A. L. Shapiro, P. W. Rooney, M. Q. Tran, F. Hellman, K. M. Ring, K. L. Kavanagh, B. Rellinghaus, and D. Weller, Phys. Rev. B **60**, 12826 (1999).

[5] J. O. Cross, M. Newville, B. B. Maranville, C. Bordel, F. Hellman, and V. G. Harris, J. Phys.: Condens. Matter **22**, 1460021 (2010).

[6] D. Treves, J. T. Jacobs, and E. Sawatzky, J. Appl. Phys. **46**, 2760 (1975).

[7] T. Shima and K. Takanashi, *Handbook of Magnetism and Advanced Magnetic Materials* (H. Kronmüller & S.-J. Parkin, Wiley, Chichester, UK, 2007), Vol. 1.

[8] Y. Yamada, T. Suzuki, H. Kanazawa, and J. C. Österman, J. Appl. Phys. **85**, 5094 (1999).

[9] S. Iwata, S. Yamashita, and S. Tsunashima, IEEE Trans. Magn. **33**, 3670 (1997).

[10] N. Mathur and P. Littlewood, Nat. Mater. **3**, 207 (2004).

[11]D. Ravelosona, C. Chappert, H. Bernas, D. Halley, Y. Samson, and A. Marty, J. Appl. Phys. **91**, 8082 (2002).
[12]H. Bernas, J.-Ph. Attane, K.-H. Heinig, D. Halley, D. Ravelosona, A. Marty, P. Auric, C. Chappert, and Y. Samson, Phys. Rev. Lett. **91**, 077203 (2003).
[13]J. Fassbender, D. Ravelosona, and Y. Samson, J. Phys. D: Appl. Phys. **37**, R179 (2004).
[14]J. Ferré and J.-P. Jamet, *Handbook on Magnetism and Advanced Magnetic Materials* (H. Kronmüller & S.-J. Parkin, Wiley, Chichester, UK, 2007), Vol. 3.
[15]T. Devolder and H. Bernas, *Material Science with Ion Beams*, edited by H. Bernas, Topics in Applied Physics, Vol. 116 (Springer-Verlag, Berlin, 2010).
[16]M. Urbaniak, P. Kuświk, Z. Kurant, M. Tekielak, D. Engel, D. Lengemann, B. Szymański, M. Schmidt, J. Aleksiejew, A. Maziewski, A. Ehresmann, and F. Stobiecki, Phys. Rev. Lett. **105**, 067202 (2010).
[17]P. Kuświk, A. Ehresmann, M. Tekielak, B. Szymański, I. Sveklo, P. Mazalski, D. Engel, J. Kisielewski, D. Lengemann, M. Urbaniak, Ch. Schmidt, A. Maziewski, and F. Stobiecki, Nanotechnology **22**, 095302 (2011).
[18]C. Chappert, H. Bernas, J. Ferré, V. Kottler, J.-P. Jamet, Y. Chen, E. Cambril, T. Devolder, F. Rousseaux, V. Mathet, and H. Launois, Science **280**, 1919 (1998).
[19]J. Fassbender and J. McCord, J. Magn. Magn. Mater. **320**, 579 (2008).
[20]C. Vieu, J. Gierak, H. Launois, T. Aign, P. Meyer, J.-P. Jamet, J. Ferré, C. Chappert, T. Devolder, V. Mathet, and H. Bernas, J. Appl. Phys. **91**, 3103 (2002).
[21]J. Jaworowicz, A. Maziewski, P. Mazalski, M. Kisielewski, I. Sveklo, M. Tekielak, V. Zablotskii, J. Ferré, N. Vernier, A. Mougin, A. Henschke, and J. Fassbender, Appl. Phys. Lett. **95**, 0225021 (2009).
[22]D. Weller, H. Brändle, and C. Chappert, J. Magn. Magn. Mater. **121**, 461 (1993).
[23]C. T. Rettner, S. Anders, J. E. E. Baglin, T. Thomson, and B. D. Terris, Appl. Phys. Lett. **80**, 279 (2002).
[24]W. Möller, W. Eckstein, and J. P. Biersack, Comp. Phys. Commun. **51**, 355 (1988).
[25]T. Devolder, S. Pizzini, J. Vogel, H. Bernas, C. Chappert, V. Mathet, and M. Borowski, Eur. Phys. J. B **22**, 193 (2001).
[26]D. Weller, G. R. Harp, R. F. C. Farrow, A. Cebollada, and J. Sticht, Phys. Rev. Lett. **72**, 2097 (1994).
[27]P. Gambardella, S. Rusponi, M. Veronese, S. Dhesi, C. Grazioli, A. Dallmeyer, I. Cabria, R. Zeller, P. H. Dederichs, K. Kern, C. Carbone, and H. Brune, Science **300**, 1130 (2003).
[28]S. Pizzini, A. Fontaine, C. Giorgetti, E. Dartyge, J.-F. Bobo, M. Piecuch, and F. Baudelet, Phys. Rev. Lett. **74**, 1470 (1995).
[29]J. Bartolomé, L. M. García, F. Bartolomé, F. Luis, R. López-Ruiz, F. Petroff, C. Deranlot, F. Wilhelm, A. Rogalev, P. Bencok, N. B. Brookes, L. Ruiz, and J. M. González-Calbet, Phys. Rev. B **77**, 184420 (2008).